THE JOURNAL OF PHYSICAL CHEMISTRY B

Article

pubs.acs.org/JPCB

Molecular Dynamics of a Water-Absorbent Nanoscale Material Based on Chitosan

Carlos H. Borca[†,‡] and Carlos A. Arango*[,‡]

[†]Departament of Chemistry, Purdue University, West Lafayette, Indiana 47907, United States

[‡]Departamento de Ciencias Químicas, Universidad Icesi, Cali, Valle del Cauca, Colombia

Supporting Information

ABSTRACT: Although hydrogels have been widely investigated for their use in materials science, nanotechnology, and novel pharmaceuticals, mechanistic details explaining their water-absorbent features are not well understood. We performed an all-atom molecular dynamics study of the structural transformation of chitosan nanohydrogels due to water absorption. We analyzed the conformation of dry, nanoscaled chitosan, the structural modifications that emerge during the process of water inclusion, and the dynamics of this biopolymer in the presence of nature's solvent. Two sets of nanoscaled, single-chained chitosan models were simulated: one to study the swelling dependence upon the degree of self-cross-linking and other to observe the response with respect to the degree of protonation. We verified that nanohydrogels keep their ability to absorb water and grow, regardless of their degree of cross-linking. Noteworthy, we found that the swelling behavior of nanoscaled chitosan is pH-dependent, and it is considerably more limited than that of larger scale hydrogels. Thus, our study suggests that properties of nanohydrogels are significantly different from those of larger hydrogels. These findings might be important in the design of novel controlled-release and targeted drug-delivery systems based on chitosan.

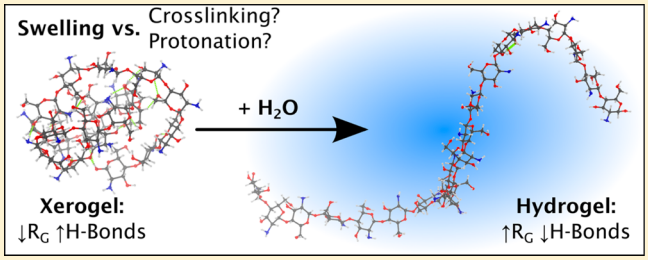

INTRODUCTION

Water-absorbent materials are one of the most exciting topics in polymer science nowadays.[1] Hydrogels are materials capable of absorbing water within networks of entangled hydrophilic polymers.[2] They are promising given their low manufacturing cost and numerous applications in science and industry.[3,4] Research in this field has expanded during the past 30 years, integrating scientists from several disciplines.[5,6]

Recently hydrogels have been used in health care and pharmaceuticals due to their unique and attractive hydrophilic, mechanical, and biocompatibility properties, which make them excellent candidates for controlled-release[7−9] and targeted drug-delivery systems.[10−13] The use of hydrogels, such as chitosan, as matrices for drugs has been employed in a considerable number of approved pharmaceutical products during the past 15 years.[14] Advances in nanotechnology have stimulated the synthesis and characterization of nanohydrogels, particles with diameters smaller than 50 nm, which might offer a number of advantages for the development of novel pharmaceuticals.[15−17] Although this is a promising research area, the literature is still limited.[18]

Chitosan is among the most common substances used to obtain macro-, micro-, and nanohydrogels.[19−23] It is a naturally occurring copolymer compounded by a variable stoichiometry of β-(1−4) D-glucosamine and its acetylated derivative, *N*-acetyl-D-glucosamine.[24,25] Its chemical structure is illustrated in atomistic detail in Figure 1.

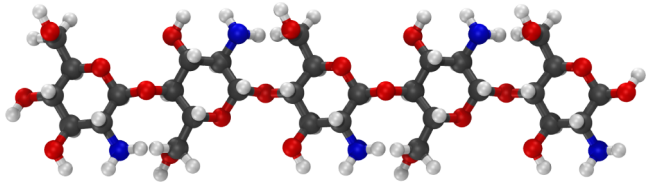

Figure 1. Extended chain of the β-(1−4) D-glucosamine pentamer. Details of the structure at the atomistic scale.

Chitosan enhances the transport of polar drugs across epithelial surfaces, and it is biocompatible and biodegradable.[6,26−29] Given their special characteristics, chitosan hydrogels have already been used in several applications: thickening agents for foods,[30] moisture releasers to plants,[31] hydrophilic coatings for textiles,[32] separation and diffusion gels in chromatography and electrophoresis,[33−35] contact lenses,[36] and as drug-delivery matrices.[6,37−40] Even though hydrogels have been widely investigated, there is a limited amount of modeling studies that discuss in detail their water-absorbent features.[6,41−43]

After the mid-1990s, the first comprehensive atomistic force fields were developed, and ever since, atomistic molecular dynamics (MD) have been taking adepts.[44] The field of

Received: November 16, 2015
Revised: January 24, 2016
Published: March 3, 2016

DOI: 10.1021/acs.jpcb.5b11230
J. Phys. Chem. B 2016, 120, 3754−3764

polymer simulations has grown hand in hand with protein modeling, and today the power of computation allows for fully atomistic description of these systems.[45] Theory and software developments for simulation of proteins have been useful for researchers in polymer science, as these two types of systems are similar.[46] Hydrogels have been studied theoretically and computationally during the past two decades.[47−50] Specifically, chitosan hydrogels have been at the center of a number of articles, most of them aiming at the optimization of synthesis and the understanding of their chemical behavior in specific types of matrices.[51−53]

Nonetheless, we have not seen a comprehensive computational study on nanohydrogels until now, especially for those based on chitosan. A few number of *in silico* research articles addressed the behavior of nanohydrogels, and in general, they are complementary to experimental work. That leaves an uncovered breach for molecular modeling studies, which is one of the motivations for this contribution.

We investigate the structural transformations that occur in model nanoscaled chitosan hydrogels when they are exposed to water. Our intention is to provide molecular insight, useful in the design of novel matrices for pharmaceutical applications. We are interested in observing the process of hydration and swelling of the polymer and any particular effects caused by the presence of nature's most common solvent. Thus, the use of all-atom MD simulations is a convenient approach to model these phenomena. We conclude that the structural properties of chitosan nanohydrogels are significantly different from those of macroscale hydrogels. Although these results should be validated by experimentation, we believe our results provide physical insights that are not obvious from the current models of hydrogels and polyelectrolytes.

COMPUTATIONAL METHODS AND SIMULATION DETAILS

MD simulations were carried out in NAMD 2.8,[54−56] using the CHARMM[57,58] force field. Reliable parametrization tools were available for NAMD, and they could be applied to cross-linked and protonated chitosan polymers, previously unparametrized.

The study was completed in two parts. In the first part, an extension of the CHARMM force field for chitosan was performed. Existing topologies and parameters for carbohydrates[59] were extended for the fully atomistic, cross-linked, and protonated chitosan models, based on quantum mechanical calculations performed on a single D-glucosamine molecule and chains with 2, 3, 4, 5, 7, and 9 β-(1−4) D-glucosamine monomers, capped with terminal methyl groups. Protonated residues were located at the center of chains with odd numbers of neutral monomers during the parametrization. Gluteraldehyde cross-links were parametrized with models that included two β-(1−4) D-glucosamine units, each one connected by their nitrogen atom to opposite sides of the cross-link. The *ab initio* calculations were executed using the GAMESS package.[60,61] First, the geometry of the systems was optimized using density functional theory with the B3LYP[62] exchange-correlation functional and Pople's 6-311G(d) basis set.[63] Tight convergence criteria for the self-consistent field procedure were applied.[64] An example of the resulting equilibrium geometry for the β-(1−4) D-glucosamine monomer is shown in Figure 2. Once the optimal geometries were obtained, single-point energy calculations were executed employing the Hartree−Fock method and the same basis set. Those included frequencies determination (Hessian matrix) and population

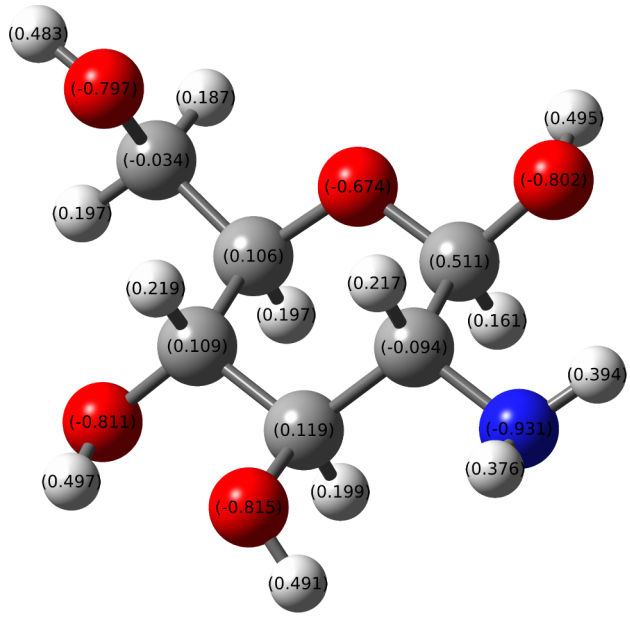

Figure 2. Optimized geometry of a β-(1−4) D-glucosamine monomer with partial ESP charges over each atom.

analysis via natural population analysis (NPA)[65] and charges fitted to the electrostatic potential (ESP) at points selected according to the Merz−Singh−Kollman scheme.[66,67] The ESP partial atomic charge distribution for the β-(1−4) D-glucosamine residue is also indicated in Figure 2. Using the *ab initio* data, missing bonding parameters were included, and the point charges were adjusted. No extra van der Waals parameters were required.

In the second part of the study, two sets of nanohydrogel models were considered, both simulated using the extended topologies and parameters. The first was designed to study the relation between the chitosan's degree of cross-linking and its swelling; thus, the chains had to be modeled in both conditions: dry and wet. A dry model would be similar to a xerogel, whereas a wet model would represent a hydrogel. The radius of gyration was used as an indicator of swelling; therefore, single-chain polymers were modeled.

This set comprised electrostatically neutral chains of 50 β-(1−4) D-glucosamine monomers with different degrees of intrachain cross-linking. The nanoscaled chitosan included nearly 1200 atoms. The longest dimension of a model in this set, measured 2.8 nm, in a dry environment. After the chains were immersed in water, the total number of atoms was close to 27 000. Following equilibration, the system including water had a average diameter of approximately 7.0 nm; thus, every model of the set could be completely surrounded by water. Models with eight different percentages of self-cross-linking were prepared: 0%, 24%, 32%, 40%, 48%, 56%, 64%, and 72%. Gluteraldehyde was chosen as the bridging molecule, a cross-linking agent commonly used in the synthesis of chitosan hydrogels.[37] The chains were radially connected, building the cross-links consecutively on top of the other, trying to keep the maximum amount of units between each cross-linked monomer, as it is illustrated in Figure 3a.

The second set of models was built to study the effect of the chain's degree of protonation on its enlargement. An example of how these models were prepared is exhibited in Figure 3b. The polymer chain included more than 450 atoms. The longest

DOI: 10.1021/acs.jpcb.5b11230
J. Phys. Chem. B 2016, 120, 3754−3764

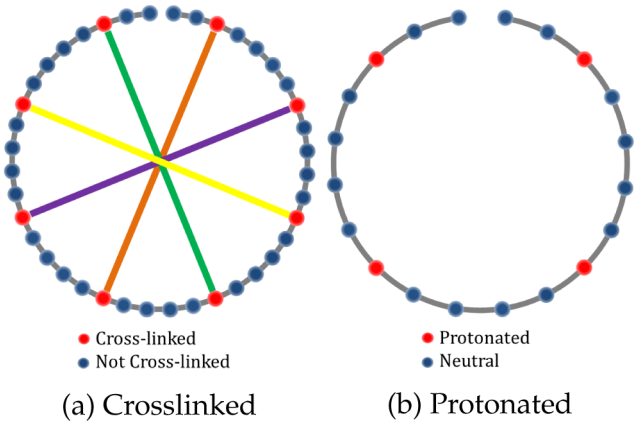

Figure 3. Schematic model of cross-linked and protonated chitosan. (a) A polymer chain with 40 monomers and 4 cross-links. (b) A polymer chain with 20 monomers and 4 protonated sites.

dimension of a model in this set measured 1.1 nm. When immersed in the solvent, the system contained around 12 000 atoms, with an average diameter of approximately 2.8 nm. This set included 20 monomers with different degrees of protonation. The most probable protonation of the β-(1−4) D-glucosamine occurs on the amine group ($-NH_2$). Hence, only the protonation of this part of the monomer was considered in our models. Instead of the amine groups, ammonium groups ($-NH_3^+$) were introduced in protonated units. The total charge of the system was balanced by adding mobile chloride (Cl^-) ions. Six chains with different percentages of protonation were created: 0%, 20%, 40%, 60%, 80%, and 100%. According to the literature, the pK_a of the amine group of chitosan is approximately 6.3.[68] These models cover a pH varying from 7.9 to 4.7, at least in theory. Though, chitosan remains stable beyond this pH range,[53] and at extreme pH conditions other functional groups start to act as acid/base pairs.

The fully atomistic representation of both sets of models is shown in Figure 4. The simulations of both sets were executed in three stages: minimization, equilibration, and production. The chain enlargement happens when water molecules reach the interior of the nanohydrogel. In order to model this process, the chains were initially simulated in a vacuum, as if they were xerogels, and then in a solvent, where the water absorption was expected to happen. As discussed previously, the first set of models were designed to study the behavior of swelling upon the degree of self-cross-linking. After building the individual chains formed by 50 monomers, their geometry was optimized in a vacuum for 10^5 steps, using the Polak-Ribière (conjugate-gradient) algorithm[69] with a root-mean-square (RMS) gradient of 1.0×10^{-6} kcal Å^{-1} mol^{-1} as convergence condition, a methodology that is suggested in the literature.[70,71] Each model was duplicated after this preliminary minimization; then, one of the copies was solvated with approximately 8000 TIP3P-type water molecules.[72] These were called the wet models. Subsequently, both dry and wet polymers were minimized again for 10^6 steps. Next, the models were equilibrated for 10 ns, performing 10^7 steps, with a time step of 1 fs/step, and using the velocity-Verlet algorithm[73] within the canonical ensemble (NVT). The temperature was controlled at 298 K using the Löwe−Andersen thermostat.[74,75] Spherical harmonic boundary conditions were applied, with an exponent of 2.0 for the boundary potential. The use of

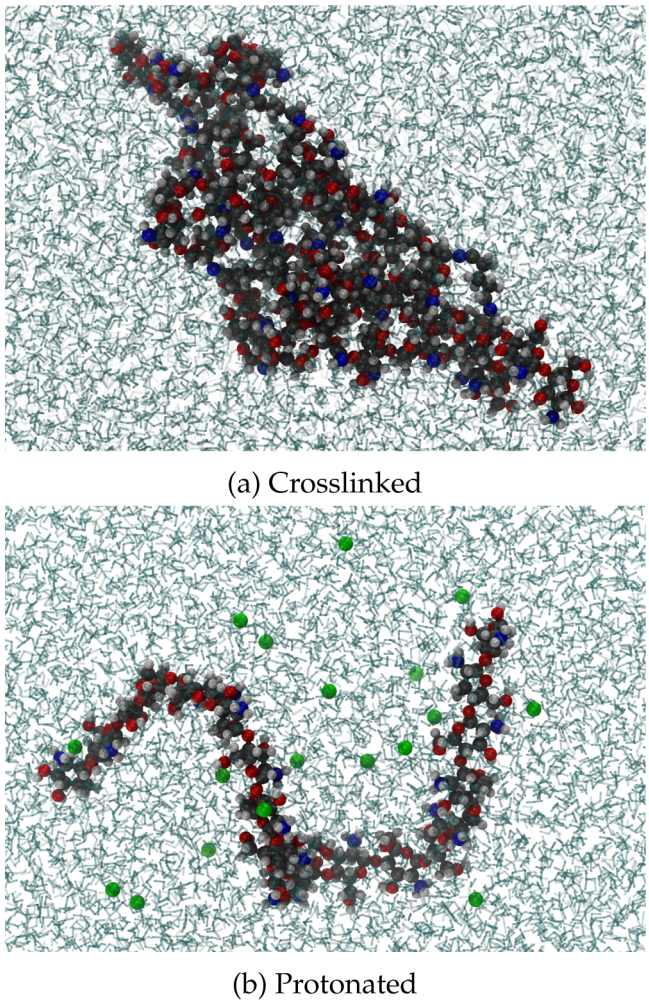

Figure 4. Atomistic models of cross-linked and protonated chitosan in water. (a) A polymer chain with 50 monomers and 18 cross-links. (b) A polymer chain with 20 monomers, 20 protonated sites, and 20 chloride counterions.

this potential implies that the system is not reproduced periodically. No initial movement of the center of masses was allowed during this stage. Bonded forces were updated at each step, short nonbonded interactions were calculated every 2 steps, and electrostatics were calculated every 4 steps. Output was written every 20 steps. Finally, after the equilibration, the production trajectories were run for 10^7 steps, of 1 fs/step, completing 10 ns.

The second set of models, designed to study swelling upon the degree of protonation, was initially minimized for 10^5 steps. Then, the chains with the solvent were prepared. These systems were smaller; they had approximately 3600 molecules of water. All of the systems were minimized, during 3×10^6 steps, using the conditions described before. Subsequently, the systems were equilibrated for 20 ns, applying the same setup: 2×10^7 steps, with a time step of 1 fs/step. Finally, the production trajectories were run for 2×10^7 steps, at a time step of 1 fs/step, completing 20 ns.

The trajectories were analyzed using VMD.[76] First, the radius of gyration, R_G, of the chain was calculated along the trajectory. R_G is a quantity used in polymer physics to describe structure and dimensions of a single-chained molecule. For an N-particle system, at any frame in the trajectory, R_G is given by

DOI: 10.1021/acs.jpcb.5b11230
J. Phys. Chem. B 2016, 120, 3754−3764

$$R_G^2 \equiv \frac{\sum_i^N m_i(\vec{r}_i - \vec{r}_{COM})^2}{\sum_i^N m_i} \quad (1)$$

where m_i and $\vec{r}_i$ are the mass and position of the ith particle, and $\vec{r}_{COM}$ is the position of the molecular center of mass. In addition, the reduced radius of gyration, $\tilde{R}_G$, is defined as

$$\tilde{R}_G \equiv \frac{R_G^{(Wet)}}{R_G^{(Solvent)}} \quad (2)$$

and it may be used to measure the size variation of a wet nanohydrogel with respect to its dry state.[77]

To extend the analysis with further chemical detail, the number of intramolecular hydrogen bonds, n_{HB}, within the polymer was calculated along the trajectory, using VMD analysis scripts. The intramolecular distinction refers to those hydrogen bonds formed between atoms of chitosan only. Hydrogen bonds with or between water atoms were excluded from the account. The algorithm considered all possible donors and acceptors within the monomers. Note that the cross-linking agent does not include any donors or acceptors. Interactions angled in excess of 35° and longer than 3.5 Å were excluded.

The net change in the average number of intramolecular hydrogen bonds, $\Delta\langle n_{HB}\rangle$, was calculated by taking the difference between the dry and wet states. This quantity was defined as

$$\Delta\langle n_{HB}\rangle \equiv \langle n_{HB}^{(Wet)}\rangle - \langle n_{HB}^{(Dry)}\rangle \quad (3)$$

RESULTS AND DISCUSSION

We analyzed the MD simulations of cross-linked and protonated chains using the time-average of $\tilde{R}_G$, and of the number of intramolecular hydrogen bonds versus the percentage of cross-linking, and of protonation for each model. We present the analyses corresponding to those four relations separately. We start with the investigation of the water-induced enlargement of chitosan nanohydrogels studying its dependence upon the degree of cross-linking, which is a tunable variable in the synthesis of these polymers.

Radius of Gyration vs degree of Theoretical Cross-Linking. Experimental determination of the percentage of cross-linked monomers is carried out using stoichiometric proportions. Thus, the exact number of chemically cross-linked monomers is unknown.[78] Furthermore, the degree of self-entanglement resulting from polymerization is also uncertain given the uncountable number of outcomes of this process.[79] Therefore, we chose our models to be chemically cross-linked and rule out self-entanglement. This approximation is attenuated by the short length of the simulated chain because the probability of self-entanglement is low.

In addition, the probability of interchain cross-linking may be higher than intrachain or self-cross-linking. However, simulating several chains in the model induces certain limitations in the analysis. For example, it requires special considerations with respect to the cross-linking pattern (radial, first neighbors, random, etc.). Also, the way in which the R_G is analyzed would depend on the cross-linking pattern. Probably a larger system would be required, too, including several chains. To avoid adding this complexity to the analysis, we designed single-chain models.

We prepared eight models to resemble different percentages of theoretical cross-linking of chitosan. We monitored their R_G along the MD trajectories. Visual inspection of the dynamics corroborated that in wet structures R_G evolved at a slower rate than in dry models. As a consequence of the presence of water, the chains tend to rearrange slower than if they were dry. Figure 5 shows a visual comparison of the final configuration of the polymers in dry and wet conditions, for each degree of cross-linking, evincing that all models swell when exposed to water.

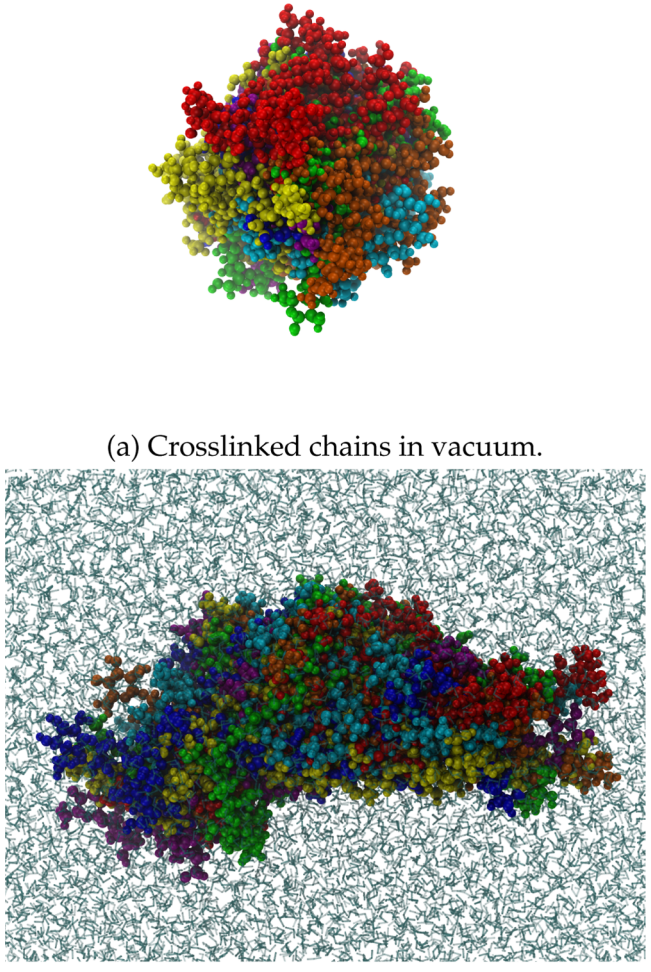

(a) Crosslinked chains in vacuum.

(b) Crosslinked chains in solvent.

Figure 5. Visualization of the structural changes induced in cross-linked chitosan chains due to the inclusion of water. There are seven superimposed models with different colors indicating their degree of cross-linking: red, 24%; orange, 32%; yellow, 40%; green, 48%; cyan, 56%; blue, 64%; and purple, 72%. Regardless of the degree of cross-linking, all the models swell when exposed to water.

Figure 6a compares R_G for dry and wet systems. Each point in this plot represents the time average of R_G during the last 5 ns of the production. We computed these averages using the R_G value at intervals of 20 steps along the trajectories. It is important to emphasize that we included the information from the statistical analyses in this graph. The shaded area is bound by the minimum and maximum values of R_G along the trajectory. The arithmetic mean is marked by the black horizontal line, accompanied by candlesticks, centered on the median, representing the standard deviation. The whisker bars mark the lower and higher quartiles, meaning that 50% of all measurements are contained within these bars. The colors on

DOI: 10.1021/acs.jpcb.5b11230
J. Phys. Chem. B 2016, 120, 3754−3764

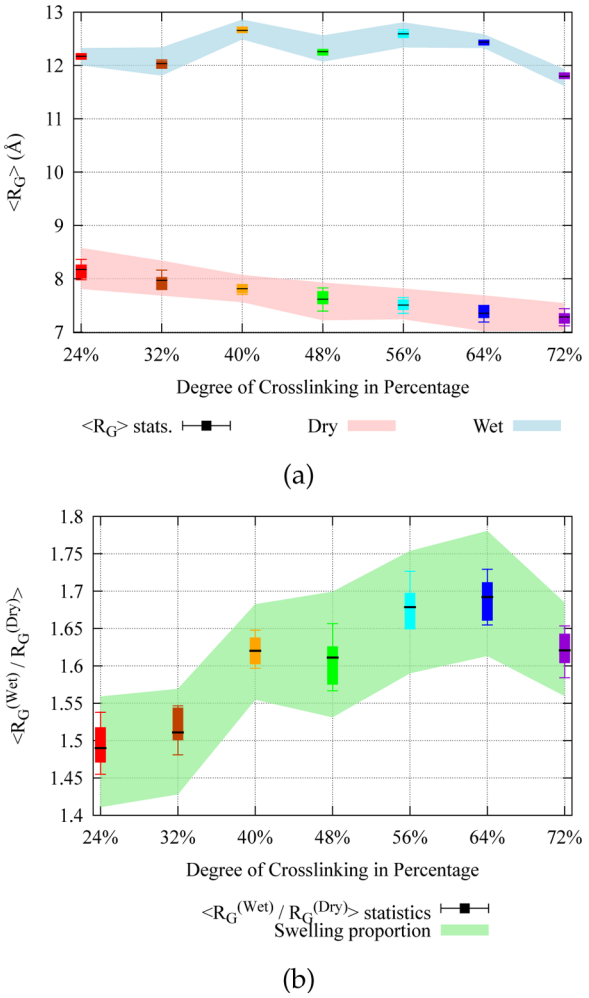

Figure 6. (a) Comparing average radius of gyration, $\langle R_G \rangle$, vs degree of cross-linking for dry and wet chains. Statistical analysis is shown: shaded area corresponds to the range of R_G; the mean is marked by a black horizontal line; candlesticks, centered on the median, represent the standard deviation; whisker bars denote the lower and higher quartiles. Dry, highly cross-linked models shrink. All systems swell when exposed to water. (b) Average reduced radius of gyration, $\langle \tilde{R}_G \rangle \equiv \langle R_G^{(Wet)}/R_G^{(Dry)} \rangle$, slightly increases with the degree of cross-linking. Statistics correspond to those of (a). Chains enlarge in water, in a range from 1.4 to 1.8 times its original $R_G^{(Dry)}$.

each bar correspond to those of the chains in Figure 5. The subsequent graphs use this notation as well.

On the one hand, Figure 6a illustrates a slightly decaying behavior of $\langle R_G \rangle$ with respect to the degree of cross-linking of dry polymers. This is because, without the solvent, high-cross-linked chains tends to be more matted than low-cross-linked models, thus yielding a shorter R_G, smaller volume, and a higher density. On the other hand, the same plot evinces an irregular behavior of $\langle R_G \rangle$ versus the degree of cross-linking for wet models. It is clear, though, that regardless of their degree of cross-linking, all models swell when hydrated.

The time-average reduced radius of gyration, $\langle \tilde{R}_G \rangle$, versus the percentage of cross-linked sites is displayed in Figure 6b, revealing that the swelling dependence of the cross-linked chains is nonlinear, although there is an increasing tendency, if the 72% trajectory is excluded. The $\langle \tilde{R}_G \rangle$ at each degree of cross-linking exhibits small relative variations, ranging from 1.4 to 1.8. In addition to the evidence discussed before, these observations lead to the conclusion that in gluteraldehyde-cross-linked chitosan nanohydrogels $\tilde{R}_G$ shows an irregular dependence upon the degree of cross-linking.

The quantitative analysis of R_G with respect to the degree of cross-linking is challenging. We prepared these models by bridging amine groups with aliphatic cross-links, but we overlooked physical entanglements that may arise naturally in small-scale hydrogels, and those might lead to smaller R_G averages. Hence, these results should be interpreted semi-quantitatively.

Nevertheless, Figure 6 proves that cross-linked nanohydrogels dilate when exposed to water, in agreement with the expectation: $\langle R_G \rangle$ increases when the chains are exposed to the solvent for each and every percentage of cross-linking. In particular, when comparing the R_G of a wet, cross-linked polymer (∼12 Å) with that of a similar wet chain without cross-links (26.31 Å), the latter is about 2 times the former. This suggests that when solvated, nonbonded intramolecular interactions of chitosan are weaker. Although the magnitude of the swelling is weakly correlated with the number of cross-linked amine groups, it is evident that when surrounded by water these nanohydrogels expand.

Summarizing, the analysis of R_G demonstrates that chitosan nanohydrogels have the ability to enlarge, as their R_G extends when exposed to water. However, the magnitude of swelling is less than expected, as compared with multiplication factors of tens or hundreds of times that macrohydrogels show.[80,81] Perhaps this is due to the inability to self-entangle and form pores or other three-dimensional structures that are involved in the process of water absorption and swelling. In contrast, it may also be an indication that gluteraldehyde is not as useful as a cross-linking agent for chitosan at this scale, as opposed to micro- and macroscaled hydrogels. In spite of that the exploration of other types of cross-links is beyond the scope of this study.

Number of Intramolecular Hydrogen Bonds vs Degree of Theoretical Cross-Linking. We also employed the time average of the number of intramolecular hydrogen bonds, $\langle n_{HB} \rangle$, to inquire into effects of water absorption in cross-linked chitosan. This analysis evaluates one of the main types of nonbonding interactions, which are crucial to understand molecular structure and dynamics in large systems. Besides, it is known that in biological or organic systems hydrogen bonding is essential in determining the conformation of solvated molecules. Moreover, several experimental and theoretical studies have claimed that hydrogen bonding is the main driving force in chitosan structural changes.[10,53]

Figure 7 comprises the results for cross-linked models. Longer standard-deviation candlesticks in Figure 7a evince that the variability of $\langle n_{HB} \rangle$ along the trajectories is more drastic than that of $\langle R_G \rangle$. Also, in contrast with what we observed during the analysis of $\langle R_G \rangle$, $\langle n_{HB} \rangle$ is closer to linearity in wet polymers as opposed to a varying behavior seen in dry polymer chains. Besides, the inspection of Figure 7a reveals an intriguing behavior in wet conditions: the most cross-linked models have the largest $\langle n_{HB} \rangle$. This implies that by keeping the monomers close to each other, cross-links enhance intramolecular interactions in wet nanohydrogels.

Figure 7b displays the net change in the average number of intramolecular hydrogen bonds, $\Delta\langle n_{HB} \rangle$, when comparing dry and wet polymers at each and every degree of cross-linking. The decrease in the amount of intramolecular hydrogen bonds is related with the degree of cross-linking of the chains. The

DOI: 10.1021/acs.jpcb.5b11230
J. Phys. Chem. B 2016, 120, 3754−3764

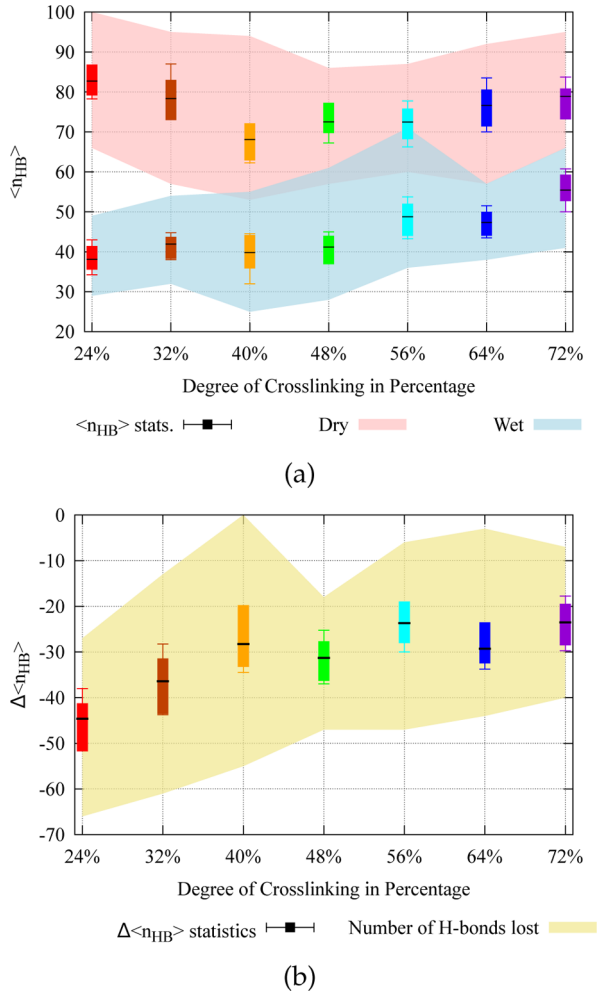

Figure 7. (a) Comparison of the average number of intramolecular hydrogen bonds, $\langle n_{HB} \rangle$, with respect to the degree of cross-linking for dry and wet chains. Statistics correspond to those of Figure 6a. Dry chains count between 68 and 84 hydrogen bonds on average. After the inclusion of water, a portion of the intramolecular hydrogen bonds are screened by water molecules and $\langle n_{HB} \rangle$ decreases. (b) Net change of the average number of intramolecular hydrogen bonds, $\Delta\langle n_{HB} \rangle$, upon the degree of cross-linking before and after the inclusion of water. In slightly cross-linked models there is a higher tendency to lose intramolecular hydrogen bonds when surrounded by water.

model with 24% cross-linked sites lost almost twice the amount of hydrogen bonds of the one with 72%. The most important observation is that $\langle n_{HB} \rangle$ is reduced with the presence of water in the surroundings of the polymers: all the models lose intramolecular hydrogen bonds when exposed to the solvent. This reveals that the interchain interactions are disrupted by solvent molecules.

Interestingly, even though $\Delta\langle n_{HB} \rangle$ is negative, meaning that intramolecular interactions are disappearing, $\langle R_G \rangle$ does not increase accordingly with respect to each degree of cross-linking (compare Figures 6b and 7b). This could indicate that other interactions, aside of hydrogen bonds, also have an important contribution to the structural modification of chitosan during water absorption. It is known that stretching, bending, and torsion forces within the chain's backbone are stronger than most nonbonding interactions, and they may limit the monomer's freedom to move during rearrangement. Also, there is experimental evidence pointing out that highly cross-linked hydrogels tend to be rather brittle, a property that is often related to stiffness of the molecular structure in these materials.[82] It is suggested that cross-links may strongly restraint motion of these short chains, so that R_G barely increases because the polymers are unable to extensively modify their configuration, and the units are forced to interact with themselves rather than with the solvent.

Notably, the hydrogen bonding analysis evinces the importance of nonbonding interactions when considering solvent effects on the structure of a biomolecule. In accordance with previous studies,[43,51,52,83] our $\Delta\langle n_{HB} \rangle$ analyses demonstrate semiquantitatively that a monomer in a wet chain loses about two or more intramolecular hydrogen bonds, offering at least two sites for hydrogen bonding with water. The great number of functional groups that are available to interact as hydrogen bond donors and acceptors is an important part in explaining the water-absorbent nature of chitosan polymers.

Both analyses highlight the influence of nonbonding interactions in the dynamics of chitosan. It is well-known that electrostatic forces are stronger than other nonbonding interactions and may be even comparable to bonding energy terms. This idea leads to inquire on how an electrostatically charged chain would interact with itself, and with water, without the restraints of a cross-link.

Radius of Gyration vs Degree of Theoretical Protonation. Experimental and theoretical studies claim that chitosan nanohydrogels are sensitive to electrostatic changes in their environments.[68,84] Additionally, pH has been used to control the swelling behavior of hydrogels.[7,10−14,37] Thus, we analyzed the effects of the protonation of monomers over the structure of a chitosan nanohydrogel. We followed the same guidelines that we used to study the incidence of the degree of cross-linking on the conformation of the chains. First, we studied the relation between R_G and the number of protonated amine groups.

Figures 8 and 9 illustrate how R_G of the dry, 20-monomer chains of chitosan depends on the amount of electrostatic charges present in the polymer or, in other words, on the percentage of protonated sites. The colors on each bar in Figure 9 correspond to those of the chains in Figure 8. All the other statistical analysis information corresponds to that of the previous graphs. A first observation with respect to the results presented in the previous subsections is that by removing the cross-links R_G increases, meaning that the chains extend.

Comparing between dry chains in Figure 9a, the data presented demonstrate that $\langle R_G \rangle$ of slightly protonated chains shortens, whereas $\langle R_G \rangle$ of highly protonated chains elongates. In addition, the $\langle R_G \rangle$ of a fully protonated dry chain is about 3 times that of the neutral. Interestingly, the size of the standard deviation increases with $\langle R_G \rangle$. This happens as a result of larger variations of R_G in highly protonated models, which could be an evidence of greater stress on the chain. This is probably related to stronger interactions between the partial electrostatic charges, increased due to closer proximity in highly protonated chains. Also, stronger electrostatics enrich the complexity of the polymer's potential energy surface, creating a variety of local minima with higher barriers between them. Thus, the system sits on these minima for longer times, creating more dispersed values of $\langle R_G \rangle$.

Figure 9b relates $\tilde{R}_G$ with the degree of protonation. The data contained within Figures 9a and 9b reveal a number of interesting facts. While the models with degree of protonation of 0%, 20%, and 40% extend when exposed to water, the ones

DOI: 10.1021/acs.jpcb.5b11230
J. Phys. Chem. B 2016, 120, 3754−3764

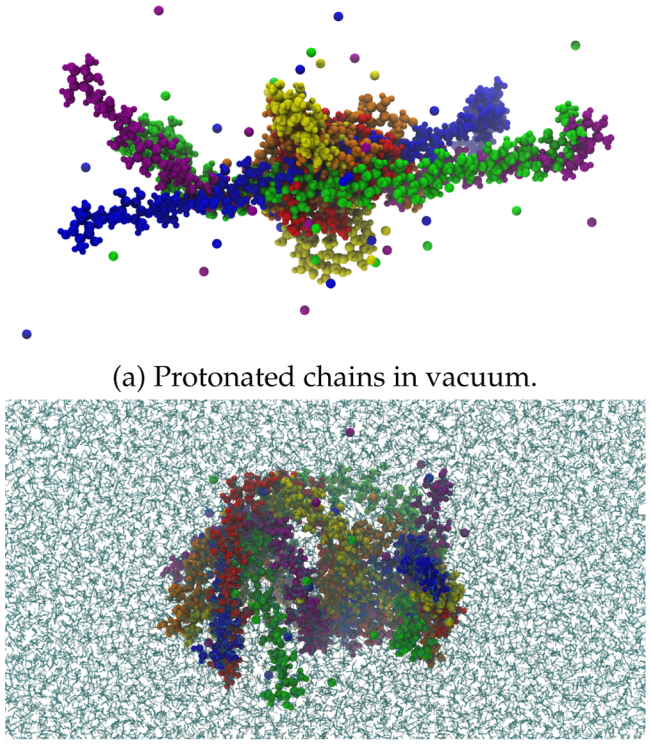

(a) Protonated chains in vacuum.

(b) Protonated chains in solvent.

Figure 8. Visualization of the structural changes induced in protonated chitosan chains due to the exposure to water. There are six superimposed models with different colors indicating the degree of protonation for each chain: red, 0%; orange, 20%; yellow, 40%; green, 60%; blue, 80%; and purple, 100%. After the inclusion of water, slightly protonated chains swell and highly protonated chains shrink.

with 60%, 80%, and 100% tend to shrink. In low-protonated chains the electrostatic forces are weak, and it is suggested that van der Waals interactions have more influence in the dynamics of the system. When the degree of protonation is high, electrostatic forces become strong enough to lead the chain's motion. However, while R_G varies between 14 and 23 Å in wet models, in the dry models it ranges from 8 to 31 Å. We think that when the solvent appears in the environment, the polymer relaxes into a conformation of intermediate R_G, given that water molecules hinder van der Waals and electrostatic intramolecular interactions.

Furthermore, Figure 9b gives a summary of the discussion above. The lesser protonated models exhibit a greater-than-one $\tilde{R}_G$, thus lengthening. The more protonated models show a less-than-one $\tilde{R}_G$, meaning they are shrinking. This type of behavior has been extensively studied before in polyelectrolyte gels and hydrogel films by the Szleifer group.[85,86] They showed that the physical properties of these gels depend on both charges regulation and molecular interactions. Our observations indicate that chitosan polymers are sensible to changes in the electrostatics of their environments, in agreement with observations found in the literature.[87] The presence of water is a determinant in the conformation of protonated chains. Thus, the swelling behavior of the chitosan nanohydrogels may be controlled by changing the pH of their environment. This feature is promising for synthesis and applications.

Although growth in slightly protonated chains is greater than in cross-linked chains, it is far from explaining size increments in the orders of hundreds shown by macroscaled hydrogels.

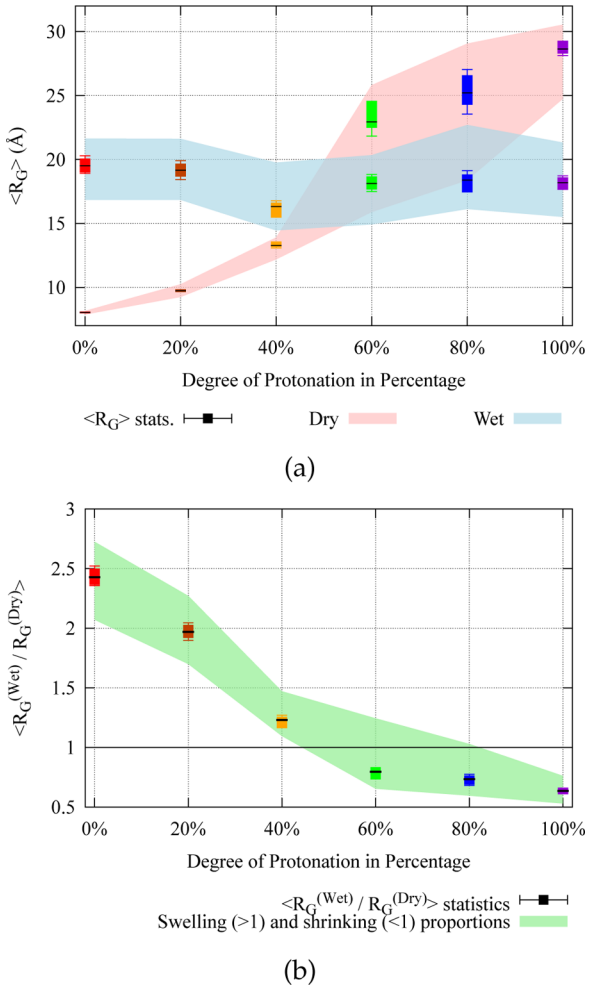

Figure 9. (a) Comparison of the average radius of gyration, $\langle R_G \rangle$, upon the degree of protonation for dry and wet chains. Statistics correspond to those of Figure 6a. Dry chains reveal an increasing tendency of $\langle R_G \rangle$ with respect to the degree of protonation: highly protonated, dry models tend to elongate. After the inclusion of water, all models show a similar, intermediate $\langle R_G \rangle$: It becomes larger for slightly protonated, wet chains and shorter for highly protonated, wet chains. (b) Reduced radius of gyration, $\langle \tilde{R}_G \rangle \equiv \langle R_G^{(Wet)}/R_G^{(Dry)} \rangle$, decreases with the degree of protonation. Slightly protonated, wet chains swell up to 2.5 times its original $R_G^{(Dry)}$, whereas highly protonated, wet chains shrink down to 0.6 times its original $R_G^{(Dry)}$. $\langle \tilde{R}_G \rangle$ is sensitive to the degree of protonation.

However, the disparity between the nano- and macroscales is significant, and the small size of our models prevents the formation of polymer networks that may exhibit these astonishing growing properties. In addition, cross-linking agents that are susceptible of being protonated may allow more swelling, given that partial electrostatic charges usually overcome van der Waals interactions and that both are diminished in the presence of water. However, the R_G analyses hint that swelling of nanohydrogels may be different than that of larger scale hydrogels.

There are several examples of the importance of nonlinear dependence of materials properties on their size. These considerations are crucial in the development of applications. Well-known examples are metallic nanoparticles: Ag, Pt, and Au are excellent catalysts for certain reactions when used as nanoparticles, while they are inert in the macroscale.[88] Another example is the very nonlinear dependence of capacitance on the

DOI: 10.1021/acs.jpcb.5b11230
J. Phys. Chem. B 2016, 120, 3754−3764

pore size of an electrode used to build supercapacitors.[89] The trends reflected in our results are an example of this type of behavior, and as such these results are important for the applied scientist.

Summarizing, this set of simulations attests that enlargement in chitosan nanohydrogels depends upon the degree of protonation. That dependence allow deprotonated chains to swell more than protonated chains. Nevertheless, when more than a half of the units are protonated, the chains deflate. This effect becomes more drastic when the degree of protonation increases. A possible explanation is that when the chain is neutral, nonbonding interactions have a significant contribution in determining the chain's motion. Then, the accumulation of partial electrostatic charges strains the polymer up to a point where electrostatics override other nonbonding forces. At this point and beyond, water screens the strong electrostatic interactions and relaxes the system, causing its shrinking. Regardless of the effects of presence of partial electrostatic charges, the increase in R_G is modest compared to the extraordinary dimensions of wet macrohydrogels, suggesting that nanohydrogels grow differently than larger scale hydrogels.

Number of Intramolecular Hydrogen Bonds vs Degree of Theoretical Protonation. Continuing the study of models with different degrees of protonation, a hydrogen bonding analysis was performed. The results are presented in Figure 10. Noteworthy, the standard deviation is similar in the distribution of data for dry or wet models.

On the one hand, Figure 10a verifies a dependence of the time-averaged number of intramolecular hydrogen bonds, $\langle n_{HB} \rangle$, upon the degree of protonation in dry conditions. There is decaying tendency, meaning that at a higher degree of protonation a smaller number of intramolecular hydrogen bonds exist. In other words, when stronger electrostatic forces appear in the system, hydrogen bonds are too weak to counteract them; therefore, they disappear and are counted out.

On the other hand, the same plot displays steady behavior of the number hydrogen bonds in relation with the degree of protonation for the wet models: $\langle n_{HB} \rangle$ remains approximately constant for all degrees of protonation. These data agree with the observations made for cross-linked chains. As in that case, both behaviors are explained by the presence of water surrounding the polymers and screening the electrostatic interactions between protonated units. However, as opposed to the previous set of simulations, in this case the nanohydrogels are unrestrained and rearrange to a conformation with a smaller $\langle n_{HB} \rangle$.

Figures 10a and 10b prove that nonprotonated and slightly protonated, dry chains have the ability to form intramolecular hydrogen bonds, whereas highly protonated, dry chains are less likely to interact with themselves in this form. This may be related with claims by experimental and *in silico* studies stating that the solubility of chitosan is pH-dependent, being soluble below 6.5 and insoluble with higher pH.[90,91] We have demonstrated that protonated chitosan nanohydrogels are less likely to establish hydrogen bond interactions with themselves. Evidently, they can be hydrophilic.

Finally, one idea connects all the results gathered in this study: both sets of systems provide evidence of swelling, though it is modest compared to that of macrohydrogels. This can only be explained, as mentioned before: nanohydrogels do not have the ability to expand as much as macrohydrogels, mainly because of their reduced size. They are unable to form networks with self-entanglements, pores, spring-shaped structures, and large vacant spaces within their three-dimensional structure. This seems to be a limiting characteristic for enlargement in nanohydrogels. Nonetheless, they are still able to absorb water and grow moderately. In addition, by modifying the pH of the environment, their size can be controlled.

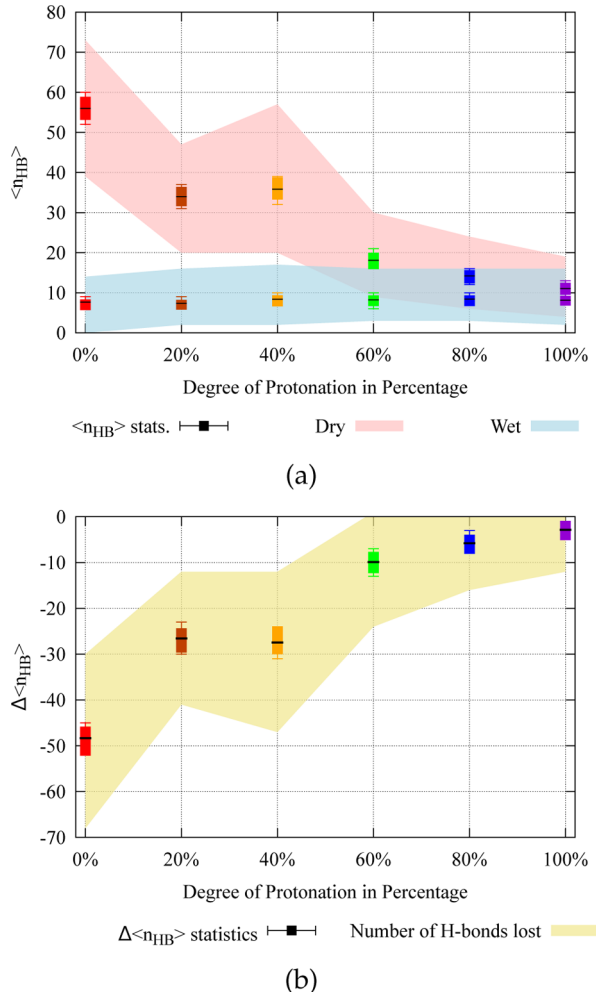

Figure 10. (a) Average number of intramolecular hydrogen bonds, $\langle n_{HB} \rangle$, in chitosan with respect to the degree of protonation for dry and wet chains. Statistics correspond to those of Figure 6a. For all degrees of protonation $\langle n_{HB} \rangle$ remains stable in wet models. Contrastingly, for dry models $\langle n_{HB} \rangle$ exhibits a decaying tendency, meaning that at a higher degree of protonation less intramolecular hydrogen bonds exist. (b) Net change of the average number of intramolecular hydrogen bonds, $\Delta\langle n_{HB} \rangle$, with respect to the degree of protonation for every protonated model. In slightly protonated models, there is a higher tendency to lose intramolecular hydrogen bonds when surrounded by water.

CONCLUSIONS

The extension of the classical force field for monomers of cross-linked and protonated chitosan exhibited its complexity: several functional groups with polarity, hydrogen bond acceptors and donors, chemically reactive sites for cross-linking agents, and protonation sites.

We demonstrated that chitosan nanohydrogels, cross-linked with gluteraldehyde bridges, extend when exposed to water. Even though it is clear that dry, highly cross-linked models show a shorter R_G, meaning a shorter average distance between monomers, we observed a nonlinear dependence of R_G upon

DOI: 10.1021/acs.jpcb.5b11230
J. Phys. Chem. B 2016, 120, 3754−3764

the degree of cross-linking, pointing out that swelling does not strictly correlate with degree of cross-linking.

The hydrogen bonding analysis of the same simulations evinced that β-(1−4) D-glucosamine monomers offer, at least, two sites for hydrogen bond interactions with other atoms of the chain or with water molecules, in accordance with the observation that chitosan is hydrophilic. Additionally, we showed that nonbonding interactions, such as hydrogen bonding and electrostatics, are essential to understand the dynamics of chitosan nanohydrogels.

Simulations with different degrees of protonation exposed the interesting nature of chitosan nanohydrogels. Their dynamics was driven by noncovalent forces, especially hydrogen bonding. However, electrostatic forces, such as repulsions between partially charged monomers, can be even more powerful than van der Waals interactions or hydrogen bonding. In highly protonated chains, the electrostatics were the dominant forces. Nevertheless, water molecules screened all types of intramolecular nonbonding interactions, relaxing the system. On the one hand, we showed that slightly protonated models elongate in the presence of water. On the other hand, highly protonated models tend to shrink when exposed to the solvent. Remarkably, the hydrogen bonding analysis of protonated models lead us to conclude that protonated chains are highly hydrophilic. Also, it evinced that the exposure to water molecules disrupts a large number of intramolecular hydrogen bonds within the chain.

The most important lesson is that nanohydrogels swell moderately compared to larger-scaled hydrogels. This was reflected in the scarce increment of R_G for all the simulated models. None of them reflected the impressive multiplication factors of tens or hundreds of times seen in macrohydrogels. In this regard, the most plausible explanation would be that the size of the simulated chains was short. Thus, it was almost impossible for them to self-entangle to form pores, spiral or folded structures, and other three-dimensional shapes that would allow for absorption of large quantities of water. Still, with this study we demonstrated that chitosan nanohydrogels swell, which is an important characteristic that synthetic chemists, such as drug designers, seek in this type of materials. Thereupon, it is suggested that they may be good candidates for controlled release and drug delivery systems because they offer the possibility of pH-controlled swelling.

It is challenging to model large systems of chitosan polymers, as the computational costs of the calculations greatly increase with the size of the system. Therefore, it was impractical to simulate a chitosan microhydrogel in accurate detail. We suggest that coarse-graining simulations, partially constrained atomistic models, and other techniques to reduce dimensionality may be a powerful tool to engage this problem in larger scales and explore other dependencies, such as the effects of modifying the chemical cross-link. However, nanohydrogels provide atomistic-scale insight into the water absorption properties of these polymer networks.

■ ASSOCIATED CONTENT

Supporting Information

The Supporting Information is available free of charge on the ACS Publications website at DOI: 10.1021/acs.jpcb.5b11230.

Plots showing the time dependence of the temperature, R_G, and n_{HB} (PDF)

An example of a NAMD configuration file as well as the topology and parameters files for chitosan (ZIP)

■ AUTHOR INFORMATION

Corresponding Author

*E-mail caarango@icesi.edu.co; Tel +57 (2) 555-2334, Ext. 8850; Fax +57 (2) 321-2078 (C.A.A.).

Notes

The authors declare no competing financial interest.

■ ACKNOWLEDGMENTS

The authors thank the Departamento Administrativo de Ciencia, Tecnología e Innovación (Colciencias) of the Colombian Goverment and Universidad Icesi for financial support conceded through the Jóvenes Investigadores e Innovadores - Virginia Gutiérrez de Pineda scholarship. They also thank Prof. Nora E. Valderruten and Prof. Eduardo Ruíz for their comments on this project. C.H.B. is immensely grateful to Prof. Lyudmila V. Slipchenko and Laura I. Mosquera-Giraldo for the enriching discussions. This research was supported in part through computational resources provided by Information Technology at Purdue University.

■ REFERENCES

(1) Brannon-Peppas, L.; Harland, R. S. *Absorbent Polymer Technology*; Elsevier: 2012.

(2) Hamidi, M.; Azadi, A.; Rafiei, P. Hydrogel Nanoparticles in Drug Delivery. *Adv. Drug Delivery Rev.* **2008**, *60*, 1638−1649.

(3) Peppas, N. A.; Bures, P.; Leobandung, W.; Ichikawa, H. Hydrogels in Pharmaceutical Formulations. *Eur. J. Pharm. Biopharm.* **2000**, *50*, 27−46.

(4) Chiessi, E.; Cavalieri, F.; Paradossi, G. Water and Polymer Dynamics in Chemically Cross-linked Hydrogels of Poly (Vinyl Alcohol): A Molecular Dynamics Simulation Study. *J. Phys. Chem. B* **2007**, *111*, 2820−2827.

(5) Tanaka, T.; Fillmore, D. J. Kinetics of Swelling of Gels. *J. Chem. Phys.* **1979**, *70*, 1214−1218.

(6) Yazdani-Pedram, M.; Tapia, C.; Retuert, J.; Arias, J. L. Synthesis and Unusual Swelling Behavior of Combined Cationic/Non-Ionic Hydrogels Based on Chitosan. *Macromol. Biosci.* **2003**, *3*, 577−581.

(7) Gupta, P.; Vermani, K.; Garg, S. Hydrogels: From Controlled Release to pH-responsive Drug Delivery. *Drug Discovery Today* **2002**, *7*, 569−579.

(8) Lin, C.-C.; Metters, A. T. Hydrogels in Controlled Release Formulations: Network Design and Mathematical Modeling. *Adv. Drug Delivery Rev.* **2006**, *58*, 1379−1408.

(9) Chang, C.; Duan, B.; Cai, J.; Zhang, L. Superabsorbent Hydrogels Based on Cellulose for Smart Swelling and Controllable Delivery. *Eur. Polym. J.* **2010**, *46*, 92−100.

(10) Qu, X.; Wirsén, A.; Albertsson, A.-C. Structural Change and Swelling Mechanism of pH-sensitive Hydrogels Based on Chitosan and D, L-lactic acid. *J. Appl. Polym. Sci.* **1999**, *74*, 3186−3192.

(11) Qiu, Y.; Park, K. Environment-sensitive Hydrogels for Drug Delivery. *Adv. Drug Delivery Rev.* **2001**, *53*, 321−339.

(12) Schmaljohann, D. Thermo- and pH-responsive Polymers in Drug Delivery. *Adv. Drug Delivery Rev.* **2006**, *58*, 1655−1670.

(13) Liu, T.-Y.; Lin, Y.-L. Novel pH-sensitive Chitosan-based Hydrogel for Encapsulating Poorly Water-soluble Drugs. *Acta Biomater.* **2010**, *6*, 1423−1429.

(14) Qu, X.; Wirsén, A.; Albertsson, A.-C. Novel pH-sensitive Chitosan Hydrogels: Swelling Behavior and States of Water. *Polymer* **2000**, *41*, 4589−4598.

(15) Sahiner, N.; Alb, A. M.; Graves, R.; Mandal, T.; McPherson, G. L.; Reed, W. F.; John, V. T. Core-shell Nanohydrogel Structures as Tunable Delivery Systems. *Polymer* **2007**, *48*, 704−711.

DOI: 10.1021/acs.jpcb.5b11230
J. Phys. Chem. B 2016, 120, 3754−3764

(16) Sahiner, N. Hydrogel Nanonetworks with Functional Core-shell Structure. *Eur. Polym. J.* **2007**, *43*, 1709−1717.
(17) Gao, D.; Xu, H.; Philbert, M. A.; Kopelman, R. Bioeliminable Nanohydrogels for Drug Delivery. *Nano Lett.* **2008**, *8*, 3320−3324.
(18) Dash, M.; Chiellini, F.; Ottenbrite, R. M.; Chiellini, E. Chitosan-A Versatile Semi-synthetic Polymer in Biomedical Applications. *Prog. Polym. Sci.* **2011**, *36*, 981−1014.
(19) Pillai, C. K. S.; Paul, W.; Sharma, C. P. Chitin and Chitosan Polymers: Chemistry, Solubility and Fiber Formation. *Prog. Polym. Sci.* **2009**, *34*, 641−678.
(20) Liu, K.-H.; Liu, T.-Y.; Chen, S.-Y.; Liu, D.-M. Drug Release Behavior of Chitosan-montmorillonite Nanocomposite Hydrogels Following Electrostimulation. *Acta Biomater.* **2008**, *4*, 1038−1045.
(21) Brunel, F.; Véron, L.; David, L.; Domard, A.; Verrier, B.; Delair, T. Self-Assemblies on Chitosan Nanohydrogels. *Macromol. Biosci.* **2010**, *10*, 424−432.
(22) Arias, J. L.; López-Viota, M.; Gallardo, V.; Adolfina Ruiz, M. Chitosan Nanoparticles as a New Delivery System for the Chemotherapy Agent Tegafur. *Drug Dev. Ind. Pharm.* **2010**, *36*, 744−750.
(23) Valderruten, N. E.; Valverde, J. D.; Zuluaga, F.; Ruiz-Durantez, E. Synthesis and Characterization of Chitosan Hydrogels Cross-linked with Dicarboxylic Acids. *React. Funct. Polym.* **2014**, *84*, 21−28.
(24) Sannan, T.; Kurita, K.; Iwakura, Y. Studies on Chitin, 1. Solubility Change by Alkaline Treatment and Film Casting. *Makromol. Chem.* **1975**, *176*, 1191−1195.
(25) Sannan, T.; Kurita, K.; Iwakura, Y. Studies on Chitin, 2. Effect of Deacetylation on Solubility. *Makromol. Chem.* **1976**, *177*, 3589−3600.
(26) Illum, L.; Farraj, N. F.; Davis, S. S. Chitosan as a Novel Nasal Delivery System for Peptide Drugs. *Pharm. Res.* **1994**, *11*, 1186−1189.
(27) Illum, L.; Jabbal-Gill, I.; Hinchcliffe, M.; Fisher, A. N.; Davis, S. S. Chitosan as a Novel Nasal Delivery System for Vaccines. *Adv. Drug Delivery Rev.* **2001**, *51*, 81−96.
(28) Thanou, M.; Verhoef, J. C.; Junginger, H. E. Oral Drug Absorption Enhancement by Chitosan and Its Derivatives. *Adv. Drug Delivery Rev.* **2001**, *52*, 117−126.
(29) Thanou, M.; Verhoef, J. C.; Junginger, H. E. Chitosan and Its Derivatives as Intestinal Absorption Enhancers. *Adv. Drug Delivery Rev.* **2001**, *50*, S91−S101.
(30) Agulló, E.; Rodríguez, M. S.; Ramos, V.; Albertengo, L. Present and Future Role of Chitin and Chitosan in Food. *Macromol. Biosci.* **2003**, *3*, 521−530.
(31) Wu, L.; Liu, M. Preparation and Properties of Chitosan-coated NPK Compound Fertilizer with Controlled-release and Water-retention. *Carbohydr. Polym.* **2008**, *72*, 240−247.
(32) Liu, B.-S.; Yao, C.-H.; Fang, S.-S. Evaluation of a Non-Woven Fabric Coated with a Chitosan Bi-Layer Composite for Wound Dressing. *Macromol. Biosci.* **2008**, *8*, 432−440.
(33) Thelen, M. P.; Delmer, D. P. Gel-electrophoretic Separation, Detection, and Characterization of Plant and Bacterial UDP-glucose Glucosyltransferases. *Plant Physiol.* **1986**, *81*, 913−918.
(34) Zeng, X.; Ruckenstein, E. Cross-linked Macroporous Chitosan Anion-exchange Membranes for Protein Separations. *J. Membr. Sci.* **1998**, *148*, 195−205.
(35) Xi, F.; Wu, J. Macroporous Chitosan Layer Coated on Non-porous Silica Gel as a Support for Metal Chelate Affinity Chromatographic Adsorbent. *Journal of Chromatography A* **2004**, *1057*, 41−47.
(36) Xin-Yuan, S.; Tian-Wei, T. New Contact Lens Based on Chitosan/Gelatin Composites. *J. Bioact. Compat. Polym.* **2004**, *19*, 467−479.
(37) Berger, J.; Reist, M.; Mayer, J. M.; Felt, O.; Peppas, N. A.; Gurny, R. Structure and Interactions in Covalently and Ionically Crosslinked Chitosan Hydrogels for Biomedical Applications. *Eur. J. Pharm. Biopharm.* **2004**, *57*, 19−34.
(38) Berger, J.; Reist, M.; Mayer, J. M.; Felt, O.; Gurny, R. Structure and Interactions in Chitosan Hydrogels Formed by Complexation or Aggregation for Biomedical Applications. *Eur. J. Pharm. Biopharm.* **2004**, *57*, 35−52.
(39) Bhattarai, N.; Gunn, J.; Zhang, M. Chitosan-based Hydrogels for Controlled, Localized Drug Delivery. *Adv. Drug Delivery Rev.* **2010**, *62*, 83−99.
(40) Muñoz, G.; Valencia, C.; Valderruten, N.; Ruiz-Durántez, E.; Zuluaga, F. Extraction of Chitosan from *Aspergillus niger* Mycelium and Synthesis of Hydrogels for Controlled Release of Betahistine. *React. Funct. Polym.* **2015**, *91*−*92*, 1−10.
(41) Müller-Plathe, F. Diffusion of Water in Swollen Poly (Vinyl Alcohol) Membranes Studied by Molecular Dynamics Simulation. *J. Membr. Sci.* **1998**, *141*, 147−154.
(42) Müller-Plathe, F. Different States of Water in Hydrogels? *Macromolecules* **1998**, *31*, 6721−6723.
(43) Sogias, I. A.; Khutoryanskiy, V. V.; Williams, A. C. Exploring the Factors Affecting the Solubility of Chitosan in Water. *Macromol. Chem. Phys.* **2010**, *211*, 426−433.
(44) Cramer, C. J. *Essentials of Computational Chemistry: Theories and Models*; Wiley: 2005.
(45) Jensen, F. *Introduction to Computational Chemistry*; Wiley: 2007.
(46) Ganji, F.; Vasheghani-Farahani, S.; Vasheghani-Farahani, E. Theoretical Description of Hydrogel Swelling: A Review. *Iran. Polym. J.* **2010**, *19*, 375−398.
(47) Tamai, Y.; Tanaka, H.; Nakanishi, K. Molecular Dynamics Study of Polymer-water Interaction in Hydrogels. 1. Hydrogen-bond Structure. *Macromolecules* **1996**, *29*, 6750−6760.
(48) Tamai, Y.; Tanaka, H.; Nakanishi, K. Molecular Dynamics Study of Polymer-water Interaction in Hydrogels. 2. Hydrogen-bond Dynamics. *Macromolecules* **1996**, *29*, 6761−6769.
(49) Tamai, Y.; Tanaka, H.; Nakanishi, K. Molecular Dynamics Study of Water in Hydrogels. *Mol. Simul.* **1996**, *16*, 359−374.
(50) Wu, C. Cooperative Behavior of Poly (Vinyl Alcohol) and Water as Revealed by Molecular Dynamics Simulations. *Polymer* **2010**, *51*, 4452−4460.
(51) Siraleartmukul, K.; Siriwong, K.; Remsungnen, T.; Muangsin, N.; Udomkichdecha, W.; Hannongbua, S. Solvation Structure of Glucosamine in Aqueous Solution as Studied by Monte Carlo Simulation Using Ab Initio Fitted Potential. *Chem. Phys. Lett.* **2004**, *395*, 233−238.
(52) Franca, E. F.; Lins, R. D.; Freitas, L. C. G.; Straatsma, T. P. Characterization of Chitin and Chitosan Molecular Structure in Aqueous Solution. *J. Chem. Theory Comput.* **2008**, *4*, 2141−2149.
(53) Franca, E. F.; Freitas, L. C. G.; Lins, R. D. Chitosan Molecular Structure as a Function of N-acetylation. *Biopolymers* **2011**, *95*, 448−460.
(54) Nelson, M.; Humphrey, W.; Kufrin, R.; Gursoy, A.; Dalke, A.; Kale, L.; Skeel, R.; Schulten, K. *Computational Mechanics 95*; Springer: 1995; pp 476−481.
(55) Kalé, L.; Skeel, R.; Bhandarkar, M.; Brunner, R.; Gursoy, A.; Krawetz, N.; Phillips, J.; Shinozaki, A.; Varadarajan, K.; Schulten, K. NAMD2: Greater Scalability for Parallel Molecular Dynamics. *J. Comput. Phys.* **1999**, *151*, 283−312.
(56) Phillips, J. C.; Braun, R.; Wang, W.; Gumbart, J.; Tajkhorshid, E.; Villa, E.; Chipot, C.; Skeel, R. D.; Kale, L.; Schulten, K. Scalable Molecular Dynamics with NAMD. *J. Comput. Chem.* **2005**, *26*, 1781−1802.
(57) Brooks, B. R.; Bruccoleri, R. E.; Olafson, B. D.; States, D. J.; Swaminathan, S.; Karplus, M. CHARMM: A Program for Macromolecular Energy, Minimization, and Dynamics Calculations. *J. Comput. Chem.* **1983**, *4*, 187−217.
(58) MacKerell, A. D.; Banavali, N.; Foloppe, N. Development and Current Status of the CHARMM Force Field for Nucleic Acids. *Biopolymers* **2000**, *56*, 257−265.
(59) Guvench, O.; Mallajosyula, S. S.; Raman, E. P.; Hatcher, E.; Vanommeslaeghe, K.; Foster, T. J.; Jamison, F. W.; MacKerell, A. D. CHARMM Additive All-Atom Force Field for Carbohydrate Derivatives and Its Utility in Polysaccharide and Carbohydrate-Protein Modeling. *J. Chem. Theory Comput.* **2011**, *7*, 3162−3180.
(60) Schmidt, M. W.; Baldridge, K. K.; Boatz, J. A.; Elbert, S. T.; Gordon, M. S.; Jensen, J. H.; Koseki, S.; Matsunaga, N.; Nguyen, K. A.;

DOI: 10.1021/acs.jpcb.5b11230
J. Phys. Chem. B 2016, 120, 3754−3764

Su, S.; et al. General Atomic and Molecular Electronic Structure System. *J. Comput. Chem.* **1993**, *14*, 1347−1363.
(61) Gordon, M. S.; Schmidt, M. W. Advances in Electronic Structure Theory: GAMESS a Decade Later. *Theory and Applications of Computational Chemistry: The First Forty Years* **2005**, 1167−1189.
(62) Becke, A. D. Density-functional Thermochemistry. III. The Role of Exact Exchange. *J. Chem. Phys.* **1993**, *98*, 5648−5652.
(63) Krishnan, R.; Binkley, J. S.; Seeger, R.; Pople, J. A. Self-consistent Molecular Orbital Methods. XX. A Basis Set for Correlated Wave Functions. *J. Chem. Phys.* **1980**, *72*, 650−654.
(64) Foresman, J. B.; Frisch, Æ. *Exploring Chemistry with Electronic Structure Methods*; Gaussian, Inc.: Pittsburgh, PA, 1996.
(65) Reed, A. E.; Weinstock, R. B.; Weinhold, F. Natural Population Analysis. *J. Chem. Phys.* **1985**, *83*, 735−746.
(66) Singh, U. C.; Kollman, P. A. An Approach to Computing Electrostatic Charges for Molecules. *J. Comput. Chem.* **1984**, *5*, 129−145.
(67) Besler, B. H.; Merz, K. M.; Kollman, P. A. Atomic Charges Derived from Semiempirical Methods. *J. Comput. Chem.* **1990**, *11*, 431−439.
(68) Park, J. W.; Choi, K.-H.; Park, K. K. Acid-base Equilibria and Related Properties of Chitosan. *Bull. Korean Chem. Soc.* **1983**, *4*, 68−72.
(69) Polak, E.; Ribière, G. Note Sur la Convergence de Méthodes de Directions Conjuguées. *ESAIM: Math. Modell. Numer. Anal.*. **1969**, *3*, 35−43.
(70) Leach, A. R. *Molecular Modelling: Principles and Applications*; Pearson Education: 2001.
(71) Lewars, E. *Computational Chemistry*; Springer: 2010.
(72) Jorgensen, W. L.; Chandrasekhar, J.; Madura, J. D.; Impey, R. W.; Klein, M. L. Comparison of Simple Potential Functions for Simulating Liquid Water. *J. Chem. Phys.* **1983**, *79*, 926−935.
(73) Swope, W. C.; Andersen, H. C.; Berens, P. H.; Wilson, K. R. A Computer Simulation Method for the Calculation of Equilibrium Constants for the Formation of Physical Clusters of Molecules: Application to Small Water Clusters. *J. Chem. Phys.* **1982**, *76*, 637−649.
(74) Lowe, C. P. An Alternative Approach to Dissipative Particle Dynamics. *Europhys. Lett.* **1999**, *47*, 145−151.
(75) Koopman, E. A.; Lowe, C. P. Advantages of a Lowe-Andersen Thermostat in Molecular Dynamics Simulations. *J. Chem. Phys.* **2006**, *124*, 204103.
(76) Humphrey, W.; Dalke, A.; Schulten, K. VMD: Visual Molecular Dynamics. *J. Mol. Graphics* **1996**, *14*, 33−38.
(77) Walter, J.; Ermatchkov, V.; Vrabec, J.; Hasse, H. Molecular Dynamics and Experimental Study of Conformation Change of Poly (N-isopropylacrylamide) Hydrogels in Water. *Fluid Phase Equilib.* **2010**, *296*, 164−172.
(78) Valentín, J. L.; Carretero-González, J.; Mora-Barrantes, I.; Chassé, W.; Saalwachter, K. Uncertainties in the Determination of Cross-link Density by Equilibrium Swelling Experiments in Natural Rubber. *Macromolecules* **2008**, *41*, 4717−4729.
(79) Arteca, G. A. Path-integral Calculation of the Mean Number of Overcrossings in an Entangled Polymer Network. *J. Chem. Inf. Model.* **1999**, *39*, 550−557.
(80) Kakuta, T.; Takashima, Y.; Harada, A. Highly Elastic Supramolecular Hydrogels Using Host-Guest Inclusion Complexes with Cyclodextrins. *Macromolecules* **2013**, *46*, 4575−4579.
(81) Sun, Y.-n.; Gao, G.-r.; Du, G.-l.; Cheng, Y.-j.; Fu, J. Super Tough, Ultrastretchable, and Thermoresponsive Hydrogels with Functionalized Triblock Copolymer Micelles as Macro-Cross-Linkers. *ACS Macro Lett.* **2014**, *3*, 496−500.
(82) Cipriano, B. H.; Banik, S. J.; Sharma, R.; Rumore, D.; Hwang, W.; Briber, R. M.; Raghavan, S. R. Superabsorbent Hydrogels That Are Robust and Highly Stretchable. *Macromolecules* **2014**, *47*, 4445−4452.
(83) Capitani, D.; Crescenzi, V.; De Angelis, A. A.; Segre, A. L. Water in Hydrogels. An NMR Study of Water/Polymer Interactions in Weakly Cross-linked Chitosan Networks. *Macromolecules* **2001**, *34*, 4136−4144.
(84) Sorlier, P.; Denuzière, A.; Viton, C.; Domard, A. Relation Between the Degree of Acetylation and the Electrostatic Properties of Chitin and Chitosan. *Biomacromolecules* **2001**, *2*, 765−772.
(85) Longo, G. S.; Olvera de la Cruz, M.; Szleifer, I. Molecular Theory of Weak Polyelectrolyte Gels: The Role of pH and Salt Concentration. *Macromolecules* **2011**, *44*, 147−158.
(86) Longo, G. S.; Olvera de la Cruz, M.; Szleifer, I. Molecular Theory of Weak Polyelectrolyte Thin Films. *Soft Matter* **2012**, *8*, 1344−1354.
(87) Hsu, L.-W.; Ho, Y.-C.; Chuang, E.-Y.; Chen, C.-T.; Juang, J.-H.; Su, F.-Y.; Hwang, S.-M.; Sung, H.-W. Effects of pH on Molecular Mechanisms of Chitosan-integrin Interactions and Resulting Tight-junction Disruptions. *Biomaterials* **2013**, *34*, 784−793.
(88) Hvolbæk, B.; Janssens, T. V.; Clausen, B. S.; Falsig, H.; Christensen, C. H.; Nørskov, J. K. Catalytic Activity of Au Nanoparticles. *Nano Today* **2007**, *2*, 14−18.
(89) Huang, Y.; Liang, J.; Chen, Y. An Overview of the Applications of Graphene-Based Materials in Supercapacitors. *Small* **2012**, *8*, 1805−1834.
(90) Kumar, M. N. V. R.; Muzzarelli, R. A. A.; Muzzarelli, C.; Sashiwa, H.; Domb, A. J. Chitosan Chemistry and Pharmaceutical Perspectives. *Chem. Rev.* **2004**, *104*, 6017−6084.
(91) Morrow, B. H.; Payne, G. F.; Shen, J. K. Titration Properties and pH-Dependent Aggregation of Chitosan. *Biophys. J.* **2015**, *108*, 488a.

DOI: 10.1021/acs.jpcb.5b11230
J. Phys. Chem. B 2016, 120, 3754−3764